SSRG International Journal of Recent Engineering Science
ISSN: 2349–7157 / https://doi.org/10.14445/23497157/IJRES-V11I4P103

Volume 11 Issue 4, 16-26, Jul-Aug 2024
© 2024 Seventh Sense Research Group®

Original Article

Comparative Performance Evaluation of Boost, Cuk and Switched Inductor DC-DC Converter using ANFIS MPPT Control for Renewable Applications

E. Kalaiyarasan[1], S. Singaravelu[2]

[1,2]*Electrical Engineering, Annamalai University, Tamilnadu, India.*

[1]*Corresponding Author : kalaiyarasan.a.m@gmail.com*

Received: 14 May 2024 Revised: 25 June 2024 Accepted: 15 July 2024 Published: 02 August 2024

Abstract - *As the demand for renewable energy sources continues to rise, Photovoltaic (PV) systems have gained significant attention as a sustainable solution for electricity generation. To maximize the efficiency and power output of standalone PV systems, effective Maximum Power Point Tracking (MPPT) techniques and efficient DC-DC converters are essential components. This study presents a comprehensive performance evaluation of three DC-DC converters, namely boost, Cuk, and a switched inductor DC-DC (SIDC) converters integrated with an Adaptive Neuro-Fuzzy Inference System (ANFIS) based MPPT control strategy for standalone PV systems. The primary objective of this research is to assess the efficiency, reliability, and overall performance of these converters under varying environmental conditions. The boost converter, known for its simplicity and widespread use, is compared with the Cuk converter, recognized for its inherent voltage inversion capability, and the innovative SIDC converter, which offers unique advantages in terms of reduced switching losses and enhanced voltage step-up capabilities. The integration of ANFIS-based MPPT control is a key aspect of this study, which aims to dynamically track the maximum power point of the PV array, further improving the overall system performance. The results of this study provide valuable insights into the performance characteristics of these converters and their suitability for standalone PV systems. Factors such as efficiency stability are analyzed, enabling system designers and researchers to make informed decisions regarding converter selection and control strategies for specific PV applications.*

Keywords - *Switched inductor DC-DC converter, ANFIS, Renewable energy, Cuk converter, Boost converter, Sustainability, Converter selection.*

1. Introduction

Growing awareness of climate change and its detrimental impacts on the planet has led to a heightened focus on reducing greenhouse gas emissions. Renewable energy sources, such as solar, wind, hydroelectric, and geothermal power, produce minimal or no greenhouse gas emissions during electricity generation, making them a crucial component of efforts to mitigate climate change [1]. Many countries are seeking to reduce their dependence on fossil fuels, which are often imported and subject to price volatility and geopolitical conflicts. By investing in domestic renewable energy sources, nations can enhance their energy security and reduce their vulnerability to energy supply disruptions [2]. The increasing global demand for renewable energy sources reflects a global shift towards cleaner, more sustainable energy options in an effort to combat climate change, enhance energy security, and drive economic growth. As the world seeks to reduce its reliance on fossil fuels and combat climate change, renewable energy sources like solar power have gained prominence. PV systems play a vital role in this transition by harnessing sunlight to generate electricity without producing greenhouse gas emissions [3]. Over the past few decades, the cost of PV technology has declined significantly. This cost reduction has made solar power more accessible and economically viable, making it an attractive option for both residential and commercial applications. PV systems provide an opportunity for individuals, businesses, and even entire regions to reduce their dependence on traditional grid-based electricity. By generating their own power, users can achieve a degree of energy independence and resilience against power outages [4]. PV systems are particularly valuable in remote or off-grid areas where extending traditional power infrastructure is expensive or impractical. Solar installations can provide electricity to communities, schools, and healthcare facilities that previously had limited access to power. Standalone Photovoltaic (PV) systems, often referred to as off-grid solar systems, have immense potential for remote and off-grid applications, playing a crucial role in providing clean and sustainable energy in areas without access to traditional power grids.

This is an open access article under the CC BY-NC-ND license (http://creativecommons.org/licenses/by-nc-nd/4.0/)

Standalone PV systems enable communities and individuals to generate their electricity independently, reducing their reliance on fossil fuels and centralized power grids. This energy independence enhances resilience and security, especially in remote areas [5]. PV systems generate electricity by harnessing sunlight, making them an environmentally friendly energy source. They produce no greenhouse gas emissions, helping combat climate change and reducing the carbon footprint of off-grid communities. Standalone PV systems can also play a crucial role in disaster-prone areas, providing a reliable source of energy for emergency response efforts, including medical facilities, communication systems, and disaster relief centers.

DC-DC converters play a crucial role in standalone photovoltaic (PV) systems by efficiently regulating and transforming voltage levels between PV panels and various system components, including loads and energy storage elements such as batteries. PV panels generate DC electricity at a specific voltage level, which varies with factors like sunlight intensity and temperature. The output voltage of PV panels is often not well-matched to the requirements of the load or the energy storage system. DC-DC converters can adjust the voltage levels to match the specific needs of the connected components. DC-DC converters can implement Maximum Power Point Tracking (MPPT) algorithms to constantly monitor the MPP and adjust the voltage and current to extract the maximum possible energy from the PV panels. This optimization ensures that the system operates at its highest efficiency, maximizing energy harvest [7]. In standalone PV systems, energy storage is crucial to provide power during periods of low sunlight or at night. DC-DC converters are used to charge batteries efficiently. They regulate the voltage and current supplied to the batteries to ensure safe and optimal charging. Loads in standalone PV systems often require specific voltage levels. DC-DC converters can adapt the PV panel output to match the voltage requirements of the connected loads. This ensures that appliances and devices receive the correct voltage and operate reliably [8]. DC-DC converters are essential components in standalone PV systems, as they optimize energy generation, storage, and usage by regulating and transforming voltage levels. Their ability to match voltage requirements, maximize energy harvest, and protect system components makes them indispensable for reliable and efficient off-grid solar power systems.

The power output of solar panels is highly dependent on various factors, including the intensity and angle of sunlight, temperature, and the electrical load connected to the panels. MPPT is a technique used to optimize the operation of PV systems to ensure they operate at their Maximum Power Point (MPP) under varying environmental conditions. MPPT controllers continuously track and adjust the operating point of the PV panels to match the MPP. By doing so, they maximize the efficiency of energy conversion, ensuring that the panels produce the most power possible given the prevailing conditions. This leads to higher energy yields and increased system efficiency [9]. Operating PV panels at their MPP reduces stress and heat generation, which can extend the lifespan of the panels. By preventing excessive current or voltage, MPPT control contributes to the reliability and durability of the PV system. Various Maximum Power Point Tracking (MPPT) control algorithms such as Perturb and Observe (P&O), Incremental Conductance (INC), Fractional Short-Circuit Current (FSCC), Hill Climbing (HC), Model Predictive Control (MPC), Artificial Neural Networks (ANN), Fuzzy Logic Control, ANFIS, Particle Swarm Optimization (PSO), Fractional Open-Circuit Voltage (FOCV), Variable Step-Size P&O (VSP&O) have been developed to optimize the efficiency of solar photovoltaic (PV) systems [10]. These algorithms are essential for ensuring that a PV system operates at its maximum power output under varying environmental conditions. One promising approach among these algorithms is the use of ANFIS. ANFIS is a hybrid intelligent system that combines the adaptability of neural networks with the interpretability of fuzzy logic. It has gained attention in the field of MPPT for its ability to adapt to changing conditions and provide accurate control. ANFIS-based MPPT algorithms work by using a combination of fuzzy logic rules and neural network learning to determine the optimal operating point of the PV system.

This work deals with the design and performance evaluation of Boost, Cuk and SIDC converters under steady and varying climatic circumstances using an optimized ANFIS MPPT control structure. In a PV system, the output voltage of the solar panel may not match the voltage required by the load or the energy storage system. The boost converter can step up the voltage to match these requirements, allowing efficient power transfer. Boost converters can operate over a wide input voltage range, making them suitable for handling variations in solar panel output due to changing weather conditions or shading. This adaptability is vital in maintaining system stability [11]. The Cuk converter is known for its ability to perform both step-up and step-down voltage conversions. This flexibility can be advantageous in standalone PV systems where the output voltage of the solar panel may vary significantly and needs to be adapted to match the load or storage system requirements. The Cuk converter can have reduced stress on components like capacitors and inductors compared to some other converter topologies [12].

The SIDC converter has the potential for high efficiency due to its unique operating principles. It is known for its reduced switching losses and improved performance compared to some other converter topologies. This can be particularly valuable in standalone PV systems where maximizing energy harvest and efficiency are serious issues. The SIDC converter is configured to provide electrical isolation between the input and output segments, which can enhance safety and protect sensitive equipment in the PV

system. The SIDC converter's operating principles lead to reduced stress on components like inductors and capacitors. This can contribute to improved reliability and durability of the converter in a PV system, reducing maintenance and replacement costs. Like other DC-DC converters mentioned in this work, the SIDC converter is integrated into ANFIS MPPT control to optimize the energy harvesting capability and efficiency of the PV system.In this paper, the DC-DC converters, namely, boost, Cuk and SIDC components, were calculated by considering the specifications of a 1KW isolated PV system. The response of the PV system is analyzed for stable and variable climatic conditions using ANFIS MPPT control for the projected converters in terms of voltage gain, mean efficiency, stability, settling time, peak overshoot and overall performance. The isolated Direct Current (DC) load is activated by employing three distinct DC-DC converters (Boost, Cuk and SIDC), each of which is integrated with an Artificial Intelligence (AI) based ANFIS MPPT tool as shown in Figure 1.

2. Literature Review

A Two-stage Switched-Capacitor DC-DC power Boost Converter has been introduced to increase the input voltage to a higher level and decrease the voltage stress on the power switch by parallel and serial configurations. Converter control methods such as fuzzy logic and PI (Proportional-Integral) are used to reduce the influence of external factors such as mechanical vibrations of the system. The output voltage, current and power of the converter are compared using fuzzy logic and PI controllers. In this work, the input voltage is directly varied (45V, 60V and 54V) instead of using PV system configurations. Duty cycle (D) variations, efficiency and voltage gain are observed. It is evidenced that the efficiency of the converter is unstable during changes in input voltages [13]. A DC-DC boost and Cuk converters are used to analyze the stability of the PV system during changes in irradiance and temperature. This analysis is carried out using the MATLAB/SIMULINK platform. In this work, the converter operation is controlled by P and O MPPT controllers. It is evidenced that the output voltages of both Boost and Cuk converters are oscillating at higher magnitudes, as shown in simulation results [14]. An adaptive perturb and observe (P&O)-fuzzy control MPPT for PV DC-DC boost converter has been projected in this work because of its simplicity and provides fast response. Performance assessment is carried out using the MATLAB/SIMULINK platform which covers overshoot, time response, oscillation and stability. Also, these results are compared with conventional P & O and conventional fuzzy logic. It is evidenced that adaptive perturb and observe (P&O)-fuzzy control response time of 15ms which is lower than other methods compared. The overshoot voltage is 0.05 volts is observed for adaptive perturb and observe (P&O)-fuzzy control and conventional fuzzy logic, and this work concludes that fuzzy is stable and adaptive perturb and observe (P&O)-fuzzy control is more stable [15].

Overall, this literature review highlights the importance of advancing control strategies for DC-DC converters in PV systems. It indicates that conventional methods may not be sufficient to address the challenges posed by varying input conditions and environmental factors. As renewable energy systems continue to play a crucial role in sustainable energy generation, further research and development in control algorithms are imperative to enhance the efficiency, stability, and overall performance of PV systems.The methodology includes the design and implementation of a projected standalone PV system consisting of a 1KW PV array, DC-DC converters (Boost, Cuk, and SIDC), ANFIS-based MPPT controller, and DC load. The ANFIS-based MPPT control strategy is implemented and integrated with each DC-DC converter. ANFIS is trained to predict the optimal operating voltage and current for maximum power extraction, utilizing historical data sets from the PV array.

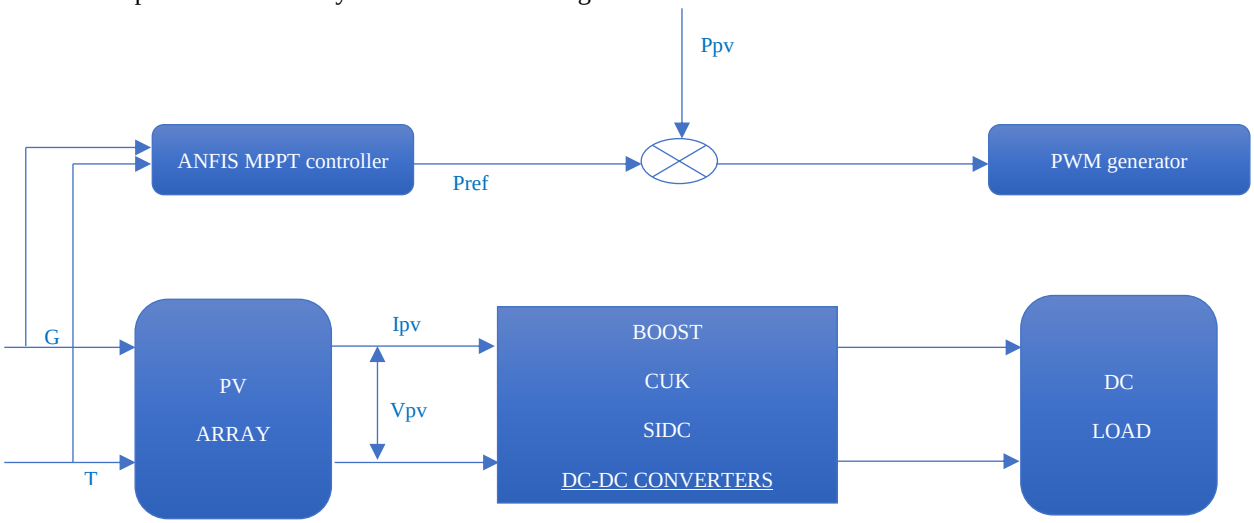

Fig. 1 Graphical abstract of the projected system

2.1. PV Array Configuration

A PV array represents the heart of any photovoltaic installation, serving as the primary source of electrical power. It is comprised of individual solar panels, each equipped with semiconductor materials that convert solar radiation into Direct Current (DC) electricity. The collective arrangement of these panels in a PV array forms a robust and scalable energy generation platform. The single diode equivalent circuit represents a PV cell/module as an electrical circuit consisting of a current source, a diode, a series resistor (R_s), and a shunt resistor (R_{sh}) connected in parallel with the diode, as shown in Figure 2.

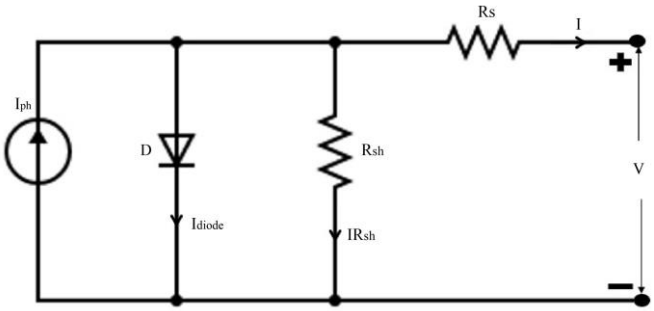

Fig. 2 Electrical equivalent circuit of the solar array

2.2. Current-Photovoltaic Current (I_{ph})

The photovoltaic current (I_{ph}) is the current generated by the PV cell/module due to sunlight. It is determined by the intensity of solar irradiance (G) and the cell/module's area (A_{cell}), as shown in Equation 1.

$$I_{ph} = G \times A_{cell} \times I_{sc} \quad (1)$$

Where:

I_{SC} is the short-circuit current of the cell/module.

2.3. Current-Diode Current (I_{diode})

The diode current (I_{diode}) represents the current passing through the diode. It depends on the cell/module's voltage (V), the diode ideality factor (n), the diode reverse saturation current (I_0), and the thermal voltage (V_T) as given in Equation 2.

$$I_{diode} = I_O(\exp \exp \left(\frac{qV}{nkT}\right) - 1) \quad (2)$$

Where:

q is the charge of an electron, k is Boltzmann's constant, T is the absolute temperature in Kelvin.

2.4. Current-Series Resistance (I_{Rs})

The series resistance (R_s) represents the resistance in series with the diode. It affects the overall performance and reduces the maximum power output. It can be determined from the voltage drop across it (V_{Rs}) and the current (I), as shown in Equation 3.

$$V_{Rs} = I * R_s \quad (3)$$

2.5. Current-Shunt Resistance (I_{Rsh})

The shunt resistance (R_{sh}) represents the resistance in parallel with the diode. It is very high in good PV modules, and thus, it does not significantly affect the performance. The total current (I) in the circuit is the sum of the photovoltaic current, diode current, and the series resistance current, as given in Equation 4.

$$\text{The total current (I)} = I_{ph} - I_{diode} - \frac{V}{R_s} + \frac{V}{R_{sh}} \quad (4)$$

Power output is calculated as the product of voltage and current as given in equation 5

$$P = I * V \quad (5)$$

In this study, the most reliable monocrystalline silicon (m-Si) solar cell-based 1KW PV array is constructed in the MATLAB/SIMULINK platform. The technical specifications of one kilowatt PV array are given in Table 1.

Table 1. PV array specifications

Parameters	Values
Open circuit voltage/cell	0.74V
Maximum voltage/cell	0.66V
Number of cells	60
Open circuit voltage /module	37.1V
Short circuit current/module	8.92A
Maximum voltage /module	29.9V
Maximum current/module	8.35A
Number of parallel strings	1
Number of series strings	4
Array Open circuit voltage	148.4V
Array Short circuit current	8.92A
Array Maximum voltage	119.6V
Array Maximum current	8.35A
Array Maximum power	998.66W

3. DC-DC Converters

3.1. Boost Converter Topology

The boost converter starts with a lower voltage input, which is typically supplied by a 1KW PV panel. The heart of the boost converter is a switching element (MOSFET), which is connected in series with the input voltage source. The inductor (L) is connected in series with the switch, which stores energy in its magnetic field when the switch is closed (ON). In parallel to the load, there is a diode which allows current to flow in one direction only, from the inductor to the output. A DC-to-DC boost converter uses the principles of energy storage and transfer to increase the input voltage to a higher output voltage.

The DC-DC boost converter output voltage can be calculated using the equation given below in reference [16],

$$V_{out} = \frac{V_{in}}{(1\text{-}D)} \quad (6)$$

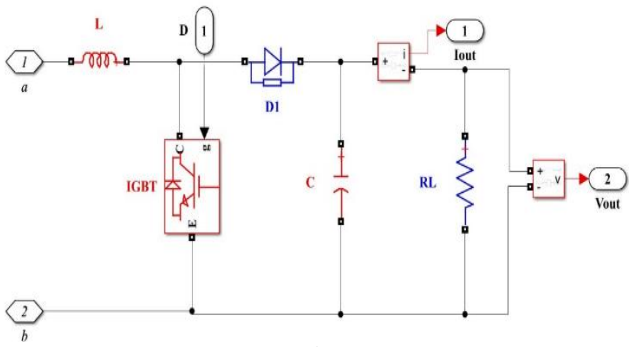

Fig. 3 Simulation diagram of DC-DC Boost converter

The required inductance value (L) for the DC-DC boost converter is determined using the following equation given below in reference [16],

$$L = \frac{R_L * D(1-D)^2}{2f} \quad (7)$$

The required output capacitance (C) for the DC-DC boost converter is determined using the following equation given below in reference [16],

$$C = \frac{V_{out} * D}{\Delta V_{out} * f * R_L} \quad (8)$$

Where ΔV_{out} is the acceptable output voltage ripple, V_{in} is the input voltage, V_{out} is the output voltage, D is the duty cycle, R_L is DC load resistance (R_L), and f is the switching frequency.

3.2. Cuk Converter Topology

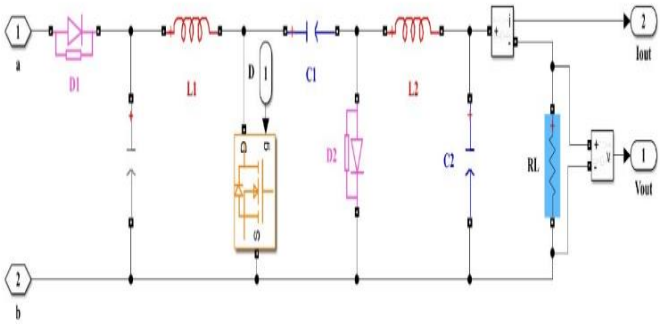

Fig. 4 Simulation diagram of Cuk converter

Figure 4 shows the simulation model of the cuk converter. The Cuk converter is a type of non-isolated topology which can perform both voltage step-up (boost) and voltage step-down (buck) operations. The inductors (L_1 & L_2) play a crucial role in energy storage and transfer. L_1 is typically used for energy storage, while L_2 transfers energy to the load. The capacitors (C_1 & C_2) are used for voltage smoothing and energy transfer. During the switch-on state, energy from the solar panel flows through L_1 and the switch to charge C_1. During the switch-off state, the stored energy in L_1 is transferred to L_2 and C_2, which are connected to the load. The voltage across C_1 is opposite in polarity to the input voltage, providing voltage inversion capability. The Cuk converter is a versatile DC-DC topology suitable for photovoltaic applications due to its efficiency, ability to step up or step down voltage, and relatively low output ripple. The average voltage of the cuk converter when it is operated in a continuous mode of operation is calculated using reference [17] as given below.

$$\frac{V_{out}}{V_{in}} = \frac{D}{(1-D)} = \text{voltage transfer ratio} \quad (9)$$

The inductors ($\Delta I_{L1} = \Delta I_{L2}$ by considering 10% of I_{out} for smoother response) and capacitors values (ΔVC_1 and (ΔVC_2 are calculated by considering 1% of V_{out}) of the cuk converter will be calculated using reference [17] as given below,

$$L_1 = \frac{(V_{in} * D)}{(\Delta I_{L1} * f)} \quad (10)$$

$$L_2 = \frac{(V_{in} * D)}{(\Delta I_{L2} * f)} \quad (11)$$

$$C_1 = \frac{(V_{out} * D)}{(\Delta V_{c1} * f * R_L)} \quad (12)$$

$$C_2 = \frac{V_{out} * (1-D)}{(8 * \Delta V_{c2} * f^2 * L_2)} \quad (13)$$

3.3. Switched Inductor DC-DC Converter Topology

The projected SIDC converter is planned to report the unique challenges faced by standalone PV systems, such as varying solar irradiance levels and load fluctuations. The key components of this converter include the two inductors (L_1 & L_2), two switches (M_1 & M_2), the input voltage source (V_{in}), two input capacitors (C_1 & C_2), the output capacitor (C_{out}), seven diodes and the output load (R_L) which work in tandem to provide efficient power conversion and regulation. Figure 4 shows the simulation model of the SIDC converter.

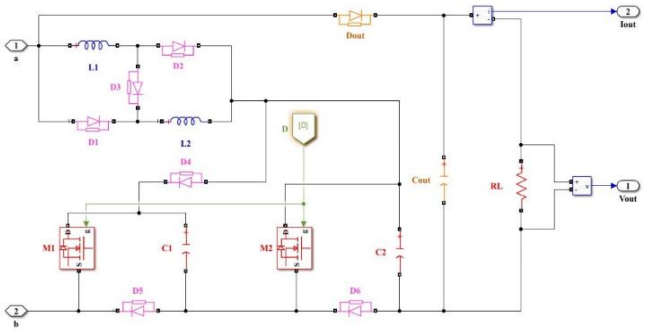

Fig 5. Simulation diagram of SIDC converter

During Mode 1, both switches M_1 and M_2 in the converter are in the ON state. Diodes D_1, D_2, and D_0 are forward-biased due to the polarity of the inductors and the input voltage source V_{in}. Inductors L_1 and L_2 are connected in parallel, allowing them to charge simultaneously. Energy is transferred to the inductors from the input voltage source, the energy stored in capacitor C_1 (VC_1), and the energy stored in capacitor

C_2 (VC_2). This energy transfer results in an increase in the current flowing through the inductors. Since L_1 and L_2 are connected in parallel and have the same voltage source, which is denoted as VL_1 and VL_2, the load connected to the converter is powered by a combination of the input voltage, the voltage across C_1 (VC_1), the voltage across C2 (VC_2).

During Mode 2, both switches M_1 and M_2 in the converter are in the OFF state. As a result, the diodes D_1, D_2, and D_0 become reverse-biased and do not conduct current. In contrast, diodes D_3, D_4, D_5, and D_6 are forward-biased and allow current to flow through them. This voltage represents the energy stored in the inductors and is an important aspect of the converter's operation. In Mode 2, both inductors L_1 and L_2 are connected in series with each other. The series configuration causes them to cooperate in discharging their stored energy. The energy stored in the inductors is dissipated into capacitors C_1 and C_2 equally during this mode. Capacitors C_1 and C_2 act as energy storage devices and absorb the energy previously stored in the inductors. During this period, the load is supplied by the energy stored in the capacitor C_{out}. Capacitor C_{out} serves as the primary source of power to the load in Mode 2. The circuit components of all three converters are designed using reference [16] [17] [18], as shown in Table 2.

The average voltage of the SIDC converter when it is operated in a continuous mode of operation is calculated using reference [18] as given below.

$$\frac{V_{out}}{V_{in}} = \frac{3-D}{(1-3D)} = \text{voltage transfer ratio} \quad (14)$$

The R_L is calculated using the $P_{out,}$ and V_{out} is given as,

$$R_L = \frac{{V_{out}}^2}{P_{out}} \quad (15)$$

The voltage across the capacitor (C_1) can be calculated as,

$$VC_1 = \frac{1+D}{1-3D} = VC_2 \quad (16)$$

Switching frequency of 100 kHz has been chosen. Now, the inductor and its current values can be calculated as given below in reference to [A. Al-Hmouz., et al., 2012],

$$L = \frac{V_{in}+VC_1}{\Delta I_L} * D * f = L_1 = L_2 \quad (17)$$

$$I_L = \frac{1}{1+D}\left(\frac{{V_{out}}^2}{V_{in}*R_L} - \frac{D*V_{out}}{R_L}\right) \quad (18)$$

The output capacitance (C_{out}) is determined by the desired voltage ripple (ΔV_{out} is calculated by considering 1% of V_{out}) and the load current (I_{out}). Let us consider a reasonable value for ΔV_{out} = 2.2V (1% of V_{out}),

$$I_{out} = \frac{P_{out}}{V_{out}} \quad (19)$$

$$C_1 = \left(\frac{2I_L+I_{out}}{\Delta VC_1}\right) D * f \quad (20)$$

$$C_2 = \left(\frac{I_{out}}{\Delta VC_2}\right) D * f \quad (21)$$

$$C_{out} = \frac{I_{out}*(1-D)}{\Delta V_{out}*f} \quad (22)$$

Table 2. Converter's component values

Components	Boost	Cuk	SIDC
L	3.56mH	13.90 µH(L_1=L_2)	19.06µH(L_1=L_2)
C_{out}	0.207F	---	0.225F
C_1	---	2.87µF	9.44µF
C_2	---	0.00105µF	101.13µF
R_L	48.4Ω		

4. Anfis Architecture & Modelling

ANFIS is a hybrid computational model that combines elements of fuzzy logic and neural networks. It is primarily used for modeling complex, nonlinear relationships between input and output data. ANFIS is a type of fuzzy inference system that adjusts its parameters through a learning process, making it capable of adapting to various types of data. The architecture of an ANFIS model typically consists of several layers [18] as follows.

4.1. Input Layer

The input layer in an ANFIS is the first component of the architecture and serves as the interface between the input data (G & T) and the ANFIS model.

Its primary function is to receive the input variables or features and pass them on to the subsequent layers for further processing.

4.2. Fuzzification Layer

In the fuzzification layer, each input value is mapped to its degree of membership in the fuzzy sets using fuzzy membership functions. The degree of membership (µ) for an input (x_i) in a fuzzy set (A_i) is calculated using the corresponding membership function (usually Gaussian); the equation for the Gaussian membership function is given as,

$$\mu(A_i) = \exp\left(-\frac{(x_i-c_i)^2}{2\sigma i^2}\right) \quad (23)$$

4.3. Rule Layer

The ruling layer combines the fuzzy membership values from the fuzzification layer to calculate the firing strength of each rule. If you have "m" rules, you will have "m" firing strengths (w_1, w_2, ..., w_m) for each rule, which can be computed using an aggregation operator (usually minimum), which is given as

$$w_i = \mu(A1_i) \times \mu(A2_i) \times \ldots\ldots \mu(An_i) \quad (24)$$

4.4. Consequent Layer

The consequent layer represents the consequences of each rule. It consists of single-layer neural networks with parameters that need to be learned. For a regression task, the output of each node in the consequent layer (y_i) can be calculated as a weighted sum of the firing strengths (w_i) with adjustable parameters (θ_i), which is given as,

$$y_i = Ø0_i + Ø1_i \times x_1 + Ø2_i \times x_2 + \cdots . Øn_i \times x_n \quad (25)$$

4.5. Output Layer

The output layer combines the outputs from the consequent layer, typically by taking their weighted sum or applying a specific aggregation method. For a single-output ANFIS, it is often a simple sum which is given as,

$$\text{output} = \frac{\epsilon(y_i \times w_i)}{\epsilon w_i} \quad [26]$$

4.6. Learning Algorithm

ANFIS uses a learning algorithm to adjust its parameters (θ_i) to minimize a predefined error or loss function. This is typically done using gradient descent or other optimization techniques. The specific equations for parameter updates depend on the chosen optimization method.

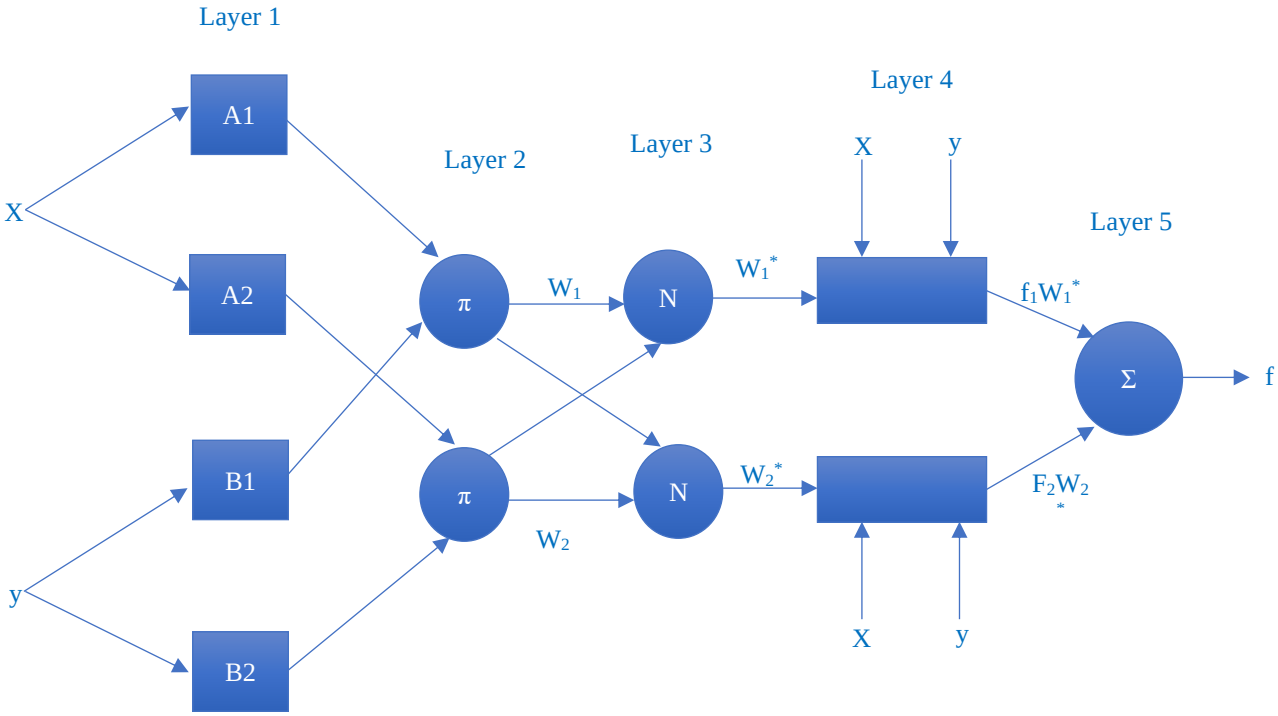

Fig. 6 ANFIS architecture

ANFIS combines the advantages of two Artificial Intelligence techniques (FLC and ANN) into a single model. An ANFIS works by implementing Artificial Neural Network learning methods to tune the parameters of a Fuzzy Inference System (FIS), and the architecture of ANFIS is given in Figure 6 [18]. This MPPT control system includes the combination of two input data sets (G and T) and output data (P_{max}). These data sets are loaded into the Neuro-fuzzy designer in MATLAB tool, as shown in Figure 7. When using the ANFIS (Adaptive Neuro-Fuzzy Inference System) tool in MATLAB, it is mandated to define the structure and configuration of FIS (Fuzzy Inference System) appropriately. This choice is crucial for achieving accurate MPPT control for the projected photovoltaic system. A 7x7 Membership Functions (MFs) configuration has been implemented in this system, which allows for a more detailed and fine-grained representation of the input variables. This can capture refined shades in the data and potentially result in more accurate modeling. Triangular MFs are selected, and it is easy to understand. They have a clear interpretation and are defined by three parameters, namely, the leftmost point, the peak, and the rightmost point. This simplicity makes it easier to design and interpret fuzzy rules for FIS.

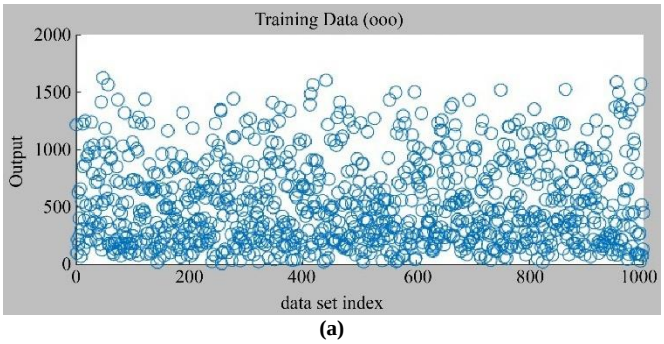

(a)

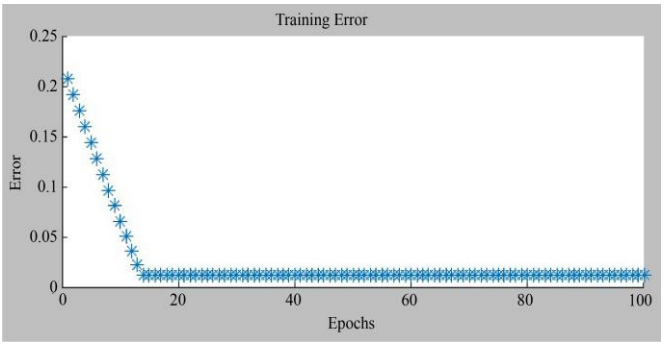

(b)

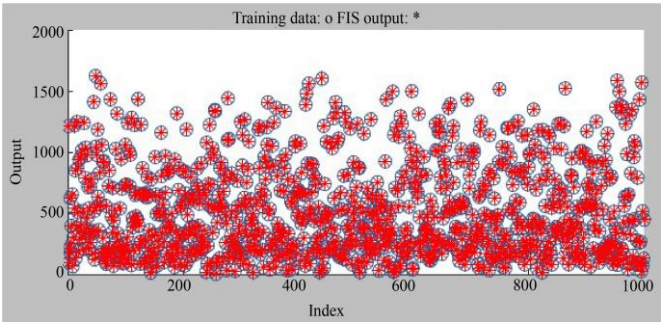

(c)

Fig. 7 (a) Input training data, (b) RMSE, (c) Output training data

In this model, nodes refer to computational units or neurons within the neural network part of the system, as shown in Figure 8. Linear parameters play a role in the weighted aggregation of fuzzy rule outputs to make a final prediction. The non-linear parameters are typically linked to MFs and determine their shapes and characteristics. The sum of the linear and nonlinear parameters is 91, which represents the overall number of adjustable parameters in the projected ANFIS model. Fuzzy rules are the core of the FIS within ANFIS. Each rule consists of antecedent conditions (if-conditions) and consequent actions (then-actions). These rules describe how input variables are combined to produce output predictions. The presence of 49 fuzzy rules indicates that the projected ANFIS model uses a relatively complex set of rules to capture system behavior. A low RMSE value (0.0132885) indicates that the ANFIS model has achieved a good fit for the training data. It means that the model's predictions are close to the actual training data values. Detailed information about the projected ANFIS model is given in Table 3.

Table 3. ANFIS training information

Sl. No	Projected ANFIS training data	
1	Number of nodes	131
2	Number of linear parameters	49
3	Number of nonlinear parameters	42
4	Total number of parameters	91
5	Number of training data pairs	1000
6	Number of fuzzy rules	49
7	Minimal training RMSE	0.0132885

5. Results and Discussion

An exhaustive examination of the performance characteristics of the Boost, Cuk and SIDC converters under diverse operating conditions such as STC, variable G & T and at variable load has been carried out using the SIMULINK model. An evaluation of the efficacy of the ANFIS MPPT control strategy in enhancing the energy harvesting capabilities of each converter was studied within the environmental scenarios. A comprehensive comparative analysis is conducted to identify the most effective combination of converter type with the projected ANFIS MPPT control across the spectrum of operating conditions.

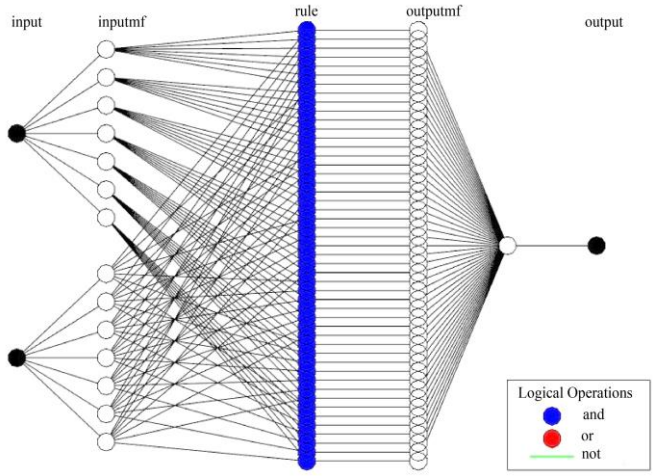

Fig. 8 Architecture of projected ANFIS model

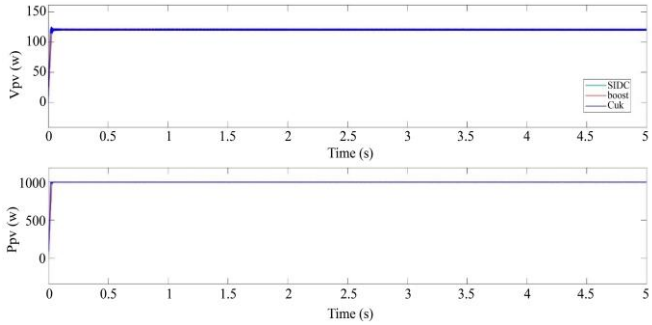

Fig. 9 Simulated PV voltage and power at STC using SIDC, Cuk and boost converters

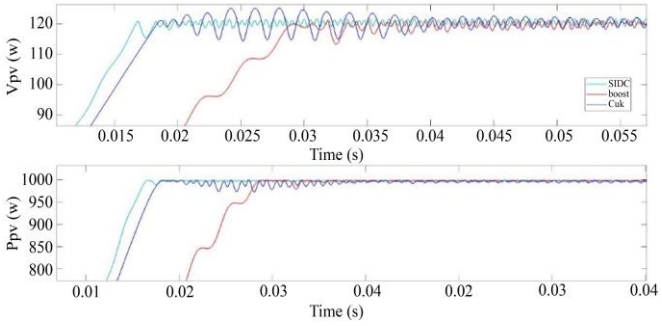

Fig. 9a Enhanced view of figure 9

Figure 9 shows the detailed representation of the V_{pv} and P_{pv} characteristics at STC, while Figure 9a shows an enhanced view of the same data. For the SIDC converter-based PV system, the Vpv is measured at 120.4V with a minor variation of 0.10V. The rise time (t_r) is observed as 12.38ms, and the settling time (t_s) was 8.94ms. Notably, this converter exhibited minimal overshoot (0.12%), and no undershoot, which proves its precise and stable performance. In the case of the Cuk converter, the PV voltage is slightly lower at 120.2V with a variation of 0.20V. The rise time was 13.93ms, and the settling time was 18.65ms. This converter demonstrated a noticeable overshoot of 1.65% and an undershoot of 5.73%, which proves that there is some transient instability in its performance. The boost converter resulted in a further reduction of PV voltage at 119.5V with a larger variation of 1.50V. Its rise time was 14.00ms, and the settling time was 24.91ms. The boost converter exhibited the highest overshoot among the three converters at 3.84%, and a substantial undershoot of 11.12%, indicating less stability and a more pronounced transient response, as shown in Table 4. The dynamic variation of temperature and irradiance are simulated by the pre-deterministic method, which is shown in Figure 10.

Table 4. Simulation analysis of PV parameters at STC

Converter type	V_{pv} (v)	ΔV_{pv} (v)	t_r (ms)	t_s (ms)	Overshoot (%)	Undershoot (%)
SIDC	120.4	0.10	12.38	8.94	0.12	0
Cuk	120.2	0.20	13.93	18.65	1.65	5.73
boost	119.5	1.50	14.00	24.91	3.84	11.12

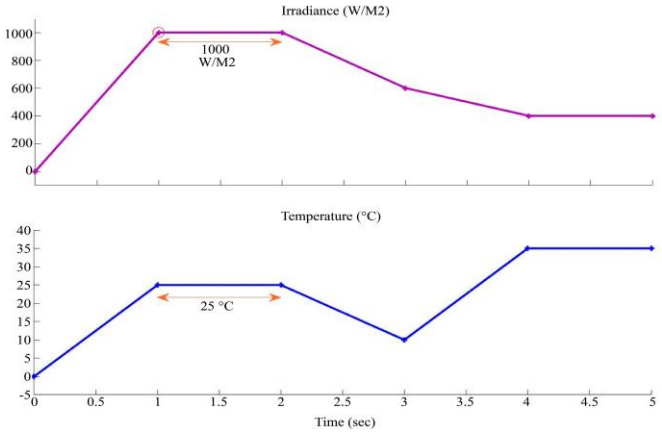

Fig. 10 Simulated variations in G and T

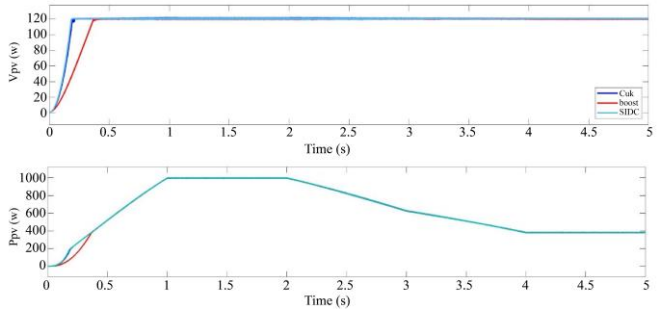

Fig. 11 Simulated PV power at variables G and T

Figure 11 shows the detailed representation of the V_{pv} characteristics using SIDC, Cuk and boost converters with ANFIS MPPT controller for variable temperature and irradiances, as shown in Figure 10. Table 5 presents the results of simulation analysis of PV parameters under varying solar irradiance and temperature conditions for the SIDC, Cuk, and boost converters. The V_{pv} remained stable at 120V with a minimal variation of 0.10V. At variable climatic conditions, t_r increased significantly to 93.21ms and the t_s extended to 180ms. There was a slight increase in both overshoot (0.12%) and undershoot (0.05%), which suggests a stable response even under changes with worst and best environmental conditions. The Cuk converter showed a lower PV voltage of 117.5V with a variation of 0.12V as G and T varied. The rise time is 122.33ms, and the settling time is observed as 193ms. This converter exhibited a greater overshoot of 3.14% and an undershot of 2.87%, which indicates some transient response challenges under variable conditions. The boost converter resulted in the lowest PV voltage at 115V with a substantial variation of 1.23V. The rise time was significantly higher at 258.04ms, and the settling time was 398ms. Under variable conditions, this converter showed a notable overshoot of 8.13% and a substantial undershoot of 21.43% which shows a significant instability in its performance under changing environmental factors. Figure 12 shows the output power of all three converters at variable environment aspects, which suggests that the P_{pv} SIDC converter is better than other converters' output power because of the SIDC converter's stable V_{pv} obtained.

Table 5. Simulation analysis of PV parameters at variable G & T

Converter type	V_{pv} (v)	ΔV_{pv} (v)	t_r (ms)	t_s (ms)	Overshoot (%)	Undershoot (%)
SIDC	120	0.10	93.21	180	0.12	0.05
Cuk	117.5	0.12	122.33	193	3.14	2.87
boost	115	1.23	258.04	398	8.13	21.43

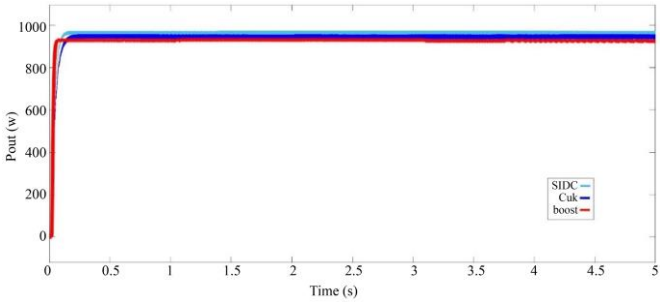

Fig. 12 Simulated Converters output power at variable G and T

Table 6. Efficiency analysis

Converter type	η_c (%) at STC	η_c (%) at variable G&T	η_c (%) at variable load
SIDC	99.7	99.2	99.4
Cuk	97.4	96.5	97.1
boost	94.6	93.8	93.5

The SIDC converter has the highest efficiency at STC (keeping load, G & T as constant values) with an impressive 99.7%, as shown in Table 6. The Cuk converter is the second most efficient at 97.4%. The boost converter has the lowest efficiency at STC, with 94.6%. The SIDC converter maintains the highest efficiency of 99.2% for random variations of G and T, as shown in Figure 10. The Cuk converter experiences a slight drop in efficiency but remains the second most efficient at 96.5%. The boost converter's efficiency drops the most significantly to 93.8%. The SIDC converter again leads with the highest efficiency of 99.4%, even under variable loads. The Cuk converter is slightly less efficient than SIDC at variable loads (97.1%). The boost converter operates for the least efficiency overall but shows a slight improvement in efficiency at variable loads (93.5%). The SIDC converter consistently proves the highest efficiency among the three converters under all conditions. It is particularly significant for maintaining high efficiency even when subjected to variations in voltage, temperature, and load.This study yields an ironic dataset that allows for a detailed examination of the performance of these converters and the influence of ANFIS MPPT control. The outcomes of this research are not only pertinent to the advancement of renewable energy systems but also offer valuable insights for researchers, engineers, and practitioners seeking to make informed decisions regarding converter selection and control strategies for their PV applications. These findings provide valuable insights into the behavior and performance characteristics of these converters in a PV system under STC and variable environment aspects, which can be instrumental for engineers and researchers in selecting the most suitable converter for specific applications.

6. Conclusion

In this comprehensive research study, we conducted an exhaustive analysis of the performance characteristics of SIDC, Cuk and boost converters under various operating conditions, which include STC, variable solar irradiance and temperature, and variable load scenarios. Also, we evaluated the efficacy of using a 7*7 linguistic member function-based ANFIS MPPT control strategy in enhancing the energy harvesting capabilities of each converter within diverse environmental scenarios. Our findings are paramount in guiding the selection of the most suitable converter type and control strategy for PV applications. At STC, it is observed that the SIDC converter has proved exceptional stability and precision with a V_{pv} of 120.4V, minimal overshoot, and no undershoot. Under variable temperature and irradiance conditions, the SIDC converter maintained a stable V_{pv} at 120V with slight increases in overshoot and undershoot. These outcomes are slightly better than the Cuk converter and the traditional boost converter fails to reach the other converter stability outcomes in an efficient manner. Furthermore, our analysis of efficiency revealed that the SIDC converter consistently outperformed the other converters under all conditions (STC, variable G & T and variable load). It achieved an impressive 99.7% efficiency at STC and maintained high efficiency even under variable solar irradiance, temperature and load conditions. The Cuk converter followed with 97.4% efficiency at STC, while the boost converter had the lowest efficiency at 94.6%. The significance of our research lies in providing a comprehensive dataset for a detailed examination of converter performance and the impact of ANFIS MPPT control. This research contributes to the understanding of converter performance in photovoltaic systems and underscores the importance of choosing the right converter type with a control strategy to optimize energy harvesting in advancing the field of renewable energy.

Acknowledgments

We gratefully acknowledge the support and facilities provided by the authorities of the Annamalai University, Annamalai Nagar, Tamilnadu, India, to carry out this research. We would also like to thank our supporting staff from Annamalai University, who provided insight and knowledge that considerably aided the research.

References

[1] David E.H.J. Gernaat et al., "Climate Change Impacts on Renewable Energy Supply," *Nature Climate Change*, vol. 11, pp. 119–125, 2021. [CrossRef] [Google Scholar] [Publisher Link]

[2] Renewables 2021, IEA. [Online]. Available: https://www.iea.org/reports/renewables-2021

[3] Dolf Gielen et al., "The Role of Renewable Energy in the Global Energy Transformation," *Energy Strategy Reviews*, vol. 24, pp. 38-50, 2019. [CrossRef] [Google Scholar] [Publisher Link]

[4] K.N. Nwaigwe, P. Mutabilwa, and E. Dintwa, "An Overview of Solar Power (PV Systems) Integration into Electricity Grids," *Materials Science for Energy Technologies*, vol. 2, no. 3, pp. 629-633, 2019. [CrossRef] [Google Scholar] [Publisher Link]

[5] Isaka J. Mwakitalima, Mohammad Rizwan, and Narendra Kumar, "Standalone Solar Photovoltaic Electricity Supply to Rural Household in Tanzania," *IETE Journal of Research*, vol. 69, no. 6, pp. 3871-3886, 2021. [CrossRef] [Google Scholar] [Publisher Link]

[6] Salahuddin Qazi, *Standalone Photovoltaic (PV) Systems for Disaster Relief and Remote Areas*, Elsevier Science, pp. 1-308, 2016. [Google Scholar] [Publisher Link]

[7] Mohammadreza Aghaei et al., "Chapter 5 - Solar PV Systems Design and Monitoring," *Photovoltaic Solar Energy Conversion*, pp. 117-145, 2020. [CrossRef] [Google Scholar] [Publisher Link]

[8] Jingyan Xie et al., "A Review of the Recent Progress of Stand-Alone Photovoltaic-battery Hybrid Energy Systems in Space and On the Ground," *Journal of Energy Storage*, vol. 55, 2022. [CrossRef] [Google Scholar] [Publisher Link]

[9] Amit Kumer Podder, Naruttam Kumar Roy, and Hemanshu Roy Pota, "MPPT Methods for Solar PV Systems: A Critical Review Based on Tracking Nature," *IET Renewable Power Generation*, vol. 13, no. 10, pp. 1615-1632, 2019. [CrossRef] [Google Scholar] [Publisher Link]

[10] Bo Yang et al., "Comprehensive Overview of Maximum Power Point Tracking Algorithms of PV Systems under Partial Shading Condition," *Journal of Cleaner Production*, vol. 268, 2020. [CrossRef] [Google Scholar] [Publisher Link]

[11] Veer Karan Goyal, and Anshuman Shukla, "Isolated DC–DC Boost Converter for Wide Input Voltage Range and Wide Load Range Applications," *IEEE Transactions on Industrial Electronics*, vol. 68, no. 10, pp. 9527-9539, 2021. [CrossRef] [Google Scholar] [Publisher Link]

[12] Carl Nelson, *5 - LT1070 Design Manual*, Analog Circuit Design, Newnes, pp. 59-123, 2011. [CrossRef] [Publisher Link]

[13] Kübra Bulut, and Davood Ertekin, "Maximum Power Point Tracking by the Small-Signal-Based PI and Fuzzy Logic Controller Approaches for a Two-Stage Switched-Capacitor DC-DC Power Boost Converter; Applicable for Photovoltaic Utilizations," *El-Cezeri*, vol. 7, no. 3, pp. 1167–1190, 2020. [CrossRef] [Google Scholar] [Publisher Link]

[14] S. Saravanan, and N. Ramesh Babu, "Performance Analysis of Boost & Cuk Converter in MPPT Based PV System," *2015 International Conference on Circuits, Power and Computing Technologies*, Nagercoil, India, pp. 1-6, 2015. [CrossRef] [Google Scholar] [Publisher Link]

[15] M.A.A. Mohd Zainuri et al., "Adaptive P&O-Fuzzy Control MPPT for PV Boost DC-DC Converter," *2012 IEEE International Conference on Power and Energy*, Kota Kinabalu, Malaysia, pp. 524-529, 2012. [CrossRef] [Google Scholar] [Publisher Link]

[16] H.A. Mohamed et al., "Design, Control and Performance Analysis of DC-DC Boost Converter for Stand-alone PV System," *2016 Eighteenth International Middle East Power Systems Conference*, Cairo, Egypt, pp. 101-106, 2016. [CrossRef] [Google Scholar] [Publisher Link]

[17] R. Sriranjani, A. ShreeBharathi, and S. Jayalalitha, "Design of Cuk Converter Powered by PV Array," *Research Journal of Applied Sciences, Engineering and Technology*, vol. 5, pp. 793-796, 2013. [CrossRef] [Publisher Link]

[18] Ahmed Al-Hmouz et al., "Modeling and Simulation of an Adaptive Neuro-Fuzzy Inference System (ANFIS) for Mobile Learning," *IEEE Transactions on Learning Technologies*, vol. 5, no. 3, pp. 226-237, 2012. [CrossRef] [Google Scholar] [Publisher Link]